Vertical migrations of fish schools determine overlap with a mobile tidal stream marine renewable energy device

Whitton, Timothy; Jackson, Suzie; Hiddink, Jan Geert; Scoulding, Ben; Bowers, David; Powell, Ben; D'Urban Jackson, Tim; Gimenez Noya, Luis; Davies, Alan

Journal of Applied Ecology

DOI:
10.1111/1365-2664.13582

Published: 01/04/2020

Peer reviewed version

Vertical migrations of fish schools determine overlap with a mobile tidal stream marine renewable energy device

Timothy A. Whitton[1]., Suzanna E. Jackson[3], Jan G. Hiddink[3] , Ben Scoulding[2], David Bowers[3], Ben Powell[3], Tim D'Urban Jackson[1], Luis Gimenez[3,4], Alan G. Davies[1],

[1]Centre for Applied Marine Sciences, Bangor University, Menai Bridge, Anglesey, LL59 5AB

[2]CSIRO Oceans & Atmosphere, Castray Esplanade Battery Point Tasmania 7004, Australia

[3]School of Ocean Sciences, Bangor University, Menai Bridge, Anglesey, LL59 5AB

[4]Biologische Anstalt Helgoland, Alfred Wegener Institute, Helmholz Centre for Polar and Marine Research, 27498, Helgoland, Germany.

Correspondence

Timothy A. Whitton

Email: t.whitton@bangor.ac.uk

Abstract

1. Large increases in the generation of electricity using marine renewable energy (MRE) are planned, and assessment of the environmental impacts of novel MRE devices, such as kites, are urgently needed. A first step in this assessment is to quantify overlap in space and time between MRE devices and prey species of top predators such as small pelagic fish.
2. Here, we quantify how the distribution of fish schools overlap with the operational depth (20–60 m) and tidal current speeds ($\geq$ 1.2 – 2.4 m s^{-1}) used by tidal kites, and the physical processes driving overlap.
2. Fish schools undertake diel vertical migrations driven by the depth of light penetration into the water column, controlled by the supply of solar radiation and water column light absorption and scattering, which in turn depends on the cross-sectional area of suspended particulate matter (SPM). Fish schools were found shallower in the morning and evening and deeper in the middle of the day when solar radiation is greatest, with the deepest depths reached during predictable bimonthly periods of lower current speeds and lower cross-sectional area of SPM.
4. Potential kite operations overlap with fish schools for a mean of 5% of the time that schools are present (maximum for a day is 36%). This represents a mean of 6% of the potential kite operating time (maximum for a day is 44%). These were both highest during a new moon spring tide and transitions between neap and spring tides.
5. *Synthesis and applications*. Overlap of fish school depth distribution with tidal kite operation is reasonably predictable, and so the timing of operations could be adapted to avoid potential negative interactions. If all interaction between fish schools was to be avoided, the loss of operational time for tidal kites would be 6%. This information could also be used in planning the operating depths of marine renewable energy (MRE) devices to avoid or minimise overlap with fish schools and their predators by developers, and for environmental licencing and management authorities to gauge potential ecological impacts of different MRE device designs and operating characteristics.

Crynodeb

1. Mae'n fwriad cynhyrchu llawer mwy o drydan yn defnyddio ynni adnewyddadwy'r môr, ac mae angen ar frys i asesu effeithiau amgylcheddol dyfeisiau newydd ynni adnewyddadwy'r môr, megis barcutiaid. Cam cyntaf yr asesiad hwn yw meintioli'r gorgyffwrdd sydd o ran amser a lle rhwng dyfeisiau ynni adnewyddadwy'r môr a'r rhywogaethau y mae'r ysglyfaethwyr pennaf yn eu bwyta megis pysgod pelagig bach.
2. I wneud hyn rydym yn meintioli sut mae dosbarthiad heigiau pysgod yn gorgyffwrdd â'r dyfnder gweithredol (20-60m) a chyflymder cerrynt y llanw ($\geq$ 1.2 - 2.4 ms^{-1}) lle gellir defnyddio barcutiaid llanw ynghyd â'r prosesau ffisegol sydd wrth wraidd y gorgyffwrdd.
3. Mae heigiau pysgod yn ymgymryd â mudo fertigol dyddiol mewn ymateb i ddyfnder treiddiad golau i'r golofn ddŵr. Yr hyn sy'n rheoli hynny yw'r cyflenwad ymbelydredd solar ac amsugnedd a gwasgariad golau yn y golofn ddŵr, sydd yn ei dro yn dibynnu ar arwynebedd trawstoriadol gronynnau (SPM) yn y dŵr. Canfuwyd heigiau pysgod mewn dŵr basach yn y bore a gyda'r nos ac mewn dŵr dyfnach ganol dydd pan fo ymbelydredd solar ar ei gryfaf, a chyrhaeddwyd y dyfnderoedd mwyaf yn ystod y cyfnodau deufisol y mae modd eu rhagweld pan fo cyflymder y cerrynt yn arafach a nifer y gronynnau yn y dŵr yn llai.
4. Mae'r cyfleoedd posib ar gyfer defnyddio barcutiaid yn gorgyffwrdd â heigiau pysgod tua 5% o'r amser, o ran cymedr, pan fo'r heigiau'n bresennol (uchafswm diwrnod yw 36%). Mae hyn yn cynrychioli cymedr o 6% o amser gweithredu posib y barcutiaid (uchafswm diwrnod yw 44%). Roedd y rhain ar eu huchaf ar lanw mawr lleuad newydd ac yn y cyfnod rhwng llanw bach a llanw mawr.
5. *Synthesis a chymwysiadau*. Mae'n rhesymol rhagweld bod gorgyffwrdd rhwng dosbarthiad dyfnder heigiau pysgod â gweithrediad barcutiaid llanw, ac felly gellid addasu pryd y cânt eu gweithredu er mwyn osgoi rhyngweithio negyddol posibl rhwng y ddau beth. Pe llwyddid i osgoi unrhyw ryngweithio â heigiau pysgod, 6% o amser gweithredol y barcutiaid llanw fyddai'n cael ei golli. Gellid defnyddio'r wybodaeth hon hefyd wrth gynllunio dyfnderoedd gweithredu dyfeisiau ynni adnewyddadwy'r môr er mwyn osgoi neu leihau'r achosion pan fo

datblygwyr yn gorgyffwrdd â heigiau pysgod, a gallai awdurdodau trwyddedu a rheoli amgylcheddol ei defnyddio i fesur effeithiau ecolegol a nodweddion gweithredu gwahanol ddyfeisiau ynni adnewyddadwy'r môr.

Keywords

Diel vertical migration, fisheries acoustics, fish schools, marine renewable energy, tidal kite, sprat, *Sprattus sprattus*, SPM

1. Introduction

Most current large-scale developments in the marine sector such as oil and gas platforms and offshore wind farms are static and do not have submerged moving parts. A new aspect of tidal marine renewable energy (MRE) devices is that they have parts, or the entire structure itself, which move through the water and at speeds up to an order of magnitude greater than the prevailing currents. This presents a need to understand the potential spatial and temporal overlap between marine fauna, such as fish (Fraser, Williamson, Nikora, & Scott, 2018; Viehman & Zydlewski, 2015) and top predators such as diving seabirds and marine mammals (Williamson et al., 2017), and mobile MRE devices.

Amongst a growing number of MRE projects in Wales UK (Roche et al., 2016), Minesto have designed and are testing a utility scale 0.5 MW bottom-tethered tidal kite (Figure 1) in the ~ 85 m deep Holyhead Deep, UK (Figure 2), with other kite systems such as SeaQurrent also in development elsewhere. The Minesto kite has a 12 m wingspan that will fly in a figure of eight pattern potentially at up to ten times the current speed between approximately 20 and 60 m depth, with plans to install an 80 MW array of kites at the site (Figure 2). Understanding prey distributions of top predators and the processes driving prey presence is required to minimize potential negative interactions of top-predators and associated prey with the tidal kites.

Despite most of the Irish Sea being tidally mixed year round, resulting in homogenous vertical distributions of phytoplankton, some groups of zooplankton undertake diel vertical migrations (DVM) (Irigoien, Conway, & Harris, 2004; Scrope-Howe & Jones, 1986). Pelagic fish such as European sprat *Sprattus sprattus*, a zooplanktivorous forage fish, change their schooling behaviour and vertical distribution during the day, schooling deep during daylight, adopting shallower depth distributions after dawn and before dusk as they vertically migrate and during darkness schools disperse (Nilsson, 2003; Solberg & Kaartvedt, 2017). In most species DVM is driven by light levels in the water column, Zooplanktivores need enough light to forage and maintain schools, but minimise predation risk by staying in as dark and deep water as possible (Bianchi & Mislan, 2016; Nilsson, 2003; Robison, 2003). Currently, there is insufficient understanding of the drivers of vertical distribution of fauna in coastal areas, and of how the high tidal current sites suitable for MRE development may influence DVM. For example, suspended particulate matter (SPM) controls turbidity by scattering and absorbing light (Granqvist & Mattila, 2004), and varies during the tidal cycle (Weeks, Simpson, & Bowers, 1993). Turbidity modifies DVM by reducing the depth of light irradiance (Lee, Kang, & Choi, 2015), which affects predation risk and other predator-prey interactions (Baptist & Leopold, 2010; De Robertis, Ryer, Veloza, & Brodeur, 2003; Kimbell & Morrell, 2015). The depth of light irradiance does not affect species equally due to reactive distance, defined as the maximum distance at which visual predators can detect prey (Vinyard & O'brien, 1976). Reactive distance is more limiting for species that feed on larger and dispersed prey than species that feed on small common prey foraged for at close ranges (De Robertis & Handegard, 2013). Therefore, through these processes, tidally driven changes in SPM, particle size and cross-sectional area (contributing to turbidity) could control animal behaviour and vertical distributions in high current areas targeted for MRE development.

Understanding the distributions of prey for diving seabirds and marine mammals should help to improve predictions of MRE device-animal interactions. Marine mammals such as porpoise (Westgate, Head, Berggren, Koopman, & Gaskin, 1995) and foraging seabirds (Baptist & Leopold, 2010; Shoji et al., 2016) have been shown to change their diving behaviour diurnally, following prey availability, and so during 24 hour periods MRE device-animal overlap may change due to diel and tidal cycles. Because

environmental regulations can limit MRE operations when seabird and marine mammal are present, understanding these interactions is not only vital for minimizing environmental impacts, but also for assessing the economic viability of MRE operations.

The aim of the study was to determine how the vertical distribution of fish schools may overlap with a tidal kite, and how key interacting physical properties of the water column such as SPM, light penetration and tidal currents drive fish school behaviour.

2. Materials and methods

2.1. Study area

The study region is macrotidal, with a semidiurnal tide reaching up to 2.7 and 1.28 m s^{-1} for mean spring peak and mean neap peak velocities respectively in the West Anglesey Demonstration Zone for tidal energy (Piano et al., 2015). The Holyhead Deep, where our study took place, is a 70 – 90 m deep depression consisting of predominantly of mixed sediments surrounded by seabed of 40 – 50 m depth just over 8 km offshore (Figure 2). With spring tide peak velocities reaching just over 2 m s^{-1}, and depths of around 85 m in the leased seabed area of 9 km^2, it is suitable for a planned development of an 80 MW array of Minesto DG500 tidal kites.

2.2. Behaviour of fish schools

2.2.1. Long term behaviour measurements

To study biological and physical processes at the site an instrumented seabed mooring system was deployed in the Holyhead Deep (Figure 2) from 1st October 2016 to 23rd January 2017. To study the vertical distribution of fish schools and other marine fauna, an upward looking four frequency (38, 67, 125, 200 kHz) factory calibrated ASL (ASL Environmental Sciences, Victoria, Canada) Acoustic Zooplankton and Fish Profiler (AZFP) was deployed on the seabed at 85 m depth (Figure 2). Multiple frequencies allowed the categorisation of targets in the water column based on their acoustic properties (Benoit-Bird & Lawson, 2016). The four frequencies pinged sequentially with a three-second interval between the four pings from the 20th of October 2016 until the mooring was recovered on 23rd January 2017.

2.2.2. Ship based sampling

To understand the spatial extent and depth distribution of fish schools in the Holyhead Deep and the representativeness of the mooring point, we carried out vessel-based echosounder transect surveys (Figure *2*) at a speed of 4 m s^{-1} using RV Prince Madog during the mooring deployment and recovery cruises. A hull mounted scientific single-beam-split-beam Simrad EK60 echosounder was used and calibrated following the methods of Demer et al. (2015). Two nominal frequencies of 38 and 120 kHz with simultaneous pinging, 512 µs pulse length and a 7 degree beam width were used. Aggregations and scattering layers observed with the EK60 were sampled using a modified 5 m^2 Oozeki mid-water trawl (Oozeki, Hu, Kubota, Sugisaki, & Kimura, 2004) with a 4.4 mm stretched mesh size (Figure 3). An ultra-short baseline underwater positioning beacon and depth logger were used to monitor trawl depth. Four trawls were taken on 5th – 6th October 2016 (during daylight), and six trawls were taken on on 22nd – 23rd January 2017 (four during darkness and two during daylight). Fast swimming adult fish such as Atlantic mackerel and adult Atlantic herring likely avoided the mid-water trawl due to the small mouth opening (5 m^2) and limited towing speed of 0.5 m s^{-1} (≈ 1 knot) through the water.

2.2.3. Processing of acoustic backscatter

Acoustic analysis of the seabed deployed AZFP backscatter focused on detecting and quantifying the depth distributions of swim-bladdered fish schools and excluded fluid-like scatterers (krill etc.) and diffuse transient layers. Vessel mounted EK60 processing also focused on detecting schools only for understanding spatial distribution within the Holyhead Deep. Both AZFP and EK60 analysis was based on the methods of Fernandes (2009) using Echoview software (Echoview Software Pty Ltd, Hobart, Australia) (Figure 4) (see Appendix S1 in supporting information).

2.3. Drivers of fish school behaviour

2.3.1.Seabed mooring

A LISST-100X (Laser *in situ* Scattering and Transmissometer-100X, Sequoia Scientific, Inc., Bellevue, USA) was deployed (Figure 2) to measure volume concentrations and size of SPM, set to log continuously in a burst mode, for one minute, with 10 second intervals and 30 minutes between bursts, from 1st October 2016 to 25th January 2017. The LISST-100X was deployed on a taught line 8 metres above the seabed. To measure current velocities a 300 kHz Teledyne RDI Workhorse Sentinel Acoustic Doppler Current Profiler (ADCP) was deployed 940 m north of the AZFP mooring (Figure 2). The distance between instruments prevented acoustic crosstalk whilst providing comparable data. The ADCP was configured in a burst mode, producing pings for four minutes every ten minutes, with five second ping intervals, in vertical depth bins of 40 cm from 1th October 2016 to 15th March 2017. Bursts were time averaged and hourly vertical current profiles calculated. Measurements closest to the instrument and the surface were removed via visual analysis due to interference at those boundaries. Current profiles were averaged over depth to calculate depth averaged current speeds (see Appendix S3).

2.3.2. Water column profiles

CTD (Conductivity, Temperature, Depth) casts profiled the water column and collected water samples for calibration of LISST-100X data. This occurred every 30 to 60 minutes over a 24-hour period during the deployment (5th – 6th October 2016) and recovery (21st – 22nd January 2017) cruises to cover different tidal periods sufficiently. A LISST-100X was mounted on the CTD to characterise vertical profiles of SPM total volume concentration (TVC) and size (D50), with a LI-COR PAR (Photosynthetically Active Radiation) sensor to measure downward-travelling irradiance in the wavelength range 400-700 nm. The estimated relationship between the irradiance and LISST-100X profiles enabled the estimated relationship between SPM properties and light absorption for the site for the entire deployment period (see section 2.3.4). The CTD and associated instruments were sampling at frequency of 1 Hz.

2.3.3. Suspended Particulate Matter Characteristics

Volume concentrations of SPM for 32 different size classes, ranging from 2.5 to 500 μm, were measured by the LISST-100X both on the seabed mooring and CTD. One minute bursts of raw volume

concentration measurements from the mooring were averaged over time, resulting in 30 minute data intervals, from which daily averages for the sampling period were calculated. For measurements from the CTD mounted LISST-100X the downward section of the profile was used. The cross-sectional area of the particles was calculated as the volume of particles in each size class, divided by the mean diameter of the particles in that class. The cross-sectional area was then summed over the 32 classes to give the total cross-sectional area of particles, *A* (units m^2 per m^3 of water of m^{-1}) for calculating the depth of light penetration (see section 2.3.4).

2.3.4. Calculating irradiance depth

Due to the importance of light in affecting the depth distribution of pelagic fauna, we predicted how the depth of light penetration changed during the study period using a new method. LI-COR PAR profiles were used to calculate the diffuse attenuation K_D for PAR, by regressing the natural logarithm of the down welling irradiance against the depth. The regression was carried out on measurements down to a depth of 10 m below the surface, or less if the irradiance was approaching the dark reading for the instrument. This gave 21 values of K_D for the two cruises applying the above criteria, ranging from 0.29 to 0.62 m^{-1} with a mean value of 0.41 m^{-1}. Assuming, in these waters, that the attenuation of light was mainly due to particles in suspension, the diffuse attenuation coefficient was plotted against total particle volume and total particle area *(A).* The relationship between K_D and particle area can be expressed as:

$$K_D = 0.202 + 0.915\ A \qquad \text{(eqn 1)}$$

with R^2 for a linear regression of 0.91 and standard errors of slope and intercept 0.064 and 0.016m^{-1} respectively. The first value (0.202 m^{-1}) represents attenuation due to water and dissolved material and the second value (0.915) the attenuation produced by particles with an area of 1m^2 in 1m^3 of water.

Equation 1 can be used to calculate the diffuse attenuation coefficient given the cross-sectional area of particles in suspension. The LISST 100X on the mooring was corrected to give the equivalent area of particles near the surface, by calculating the total area of particles in 10 m bins from the CTD profiles. For all profiles, the ratio of the average area of particles in the top bin to that in the bottom bin (the

depth of the mooring), was 0.473. The near bed total particle area data was corrected using this ratio and K_D was calculated with equation 1.

Surface global irradiance (in units of MJ m^{-2} hr^{-1}) from the meteorological station at Valley airport on Anglesey (30 km from the mooring site) was used to calculate the depth at which the irradiance reaches a 'twilight' value E_D, defined here as irradiance depth (Z), which can be calculated from the surface irradiance E_0 and the diffuse attenuation coefficient K_D, using:

$$Z = (-1/K_D) \log (E_D/E_0) \quad \text{(eqn 2)}$$

A value of E_D = 10 MJ m^{-2} hr^{-1} was used in this calculation.

2.4. Patterns and relationships between fish school depths and physical properties

The described acoustic processing of the AZFP backscatter produced a depth and time for each detected school. These were averaged by hour to help account for inter-school variation in behaviour, to match the temporal resolution of environmental variables and allow observation of daily behavioural trends, and observe multiday to monthly patterns. To test for the effect of different tidal cycles with periods of seven days (period between neap–spring tides), 14 days (neap to neap or spring to spring tides) and 29 days (N_2 harmonic lunar month of new moon to new moon) on fish school depth, time series analysis using seasonal-trend decomposition by regression was conducted using the stR package (Dokumentov & Hyndman, 2018) in R (R Core Team, 2019).

2.5. MRE device overlap

The predicted proportion of hours that DVM fish schools are overlapped by kite flying operations during a day (PO_{FS}) was defined (eq3) as the ratio of the total number of hours fish schools (*FS*) are present in a day to the total hours that fish schools are within the kite operating envelope of 20 m to 60 m depth and current velocity (*U*) 1.2 m s^{-1} to 2.4 m s^{-1}.

$$PO_{FS} = \frac{hours\ FS > 20\ m\ \&\ < 60\ m\ \&\ U > 1.2\ m\ s^{-1}\ \&\ < 2.4\ m\ s^{-1}}{hours\ FS\ present} \quad \text{(eqn3)}$$

The predicted daily proportion of kite operation hours in a day overlapped by DVM fish schools (PO_k) was defined (eq4) as the ratio of the total hours when the kite is operating as determined by the current

velocity, to the hours that fish schools are also present in the kite operating depth and kite operating current velocities (eq4).

$$PO_k = \frac{hours\ FS > 20\ m\ \&\ < 60\ m\ \&\ U > 1.2\ m\ s^{-1}\ \&\ < 2.4\ m\ s^{-1}}{hours\ U > 1.2\ m\ s^{-1}\ \&\ < 2.4\ m\ s^{-1}} \quad \text{(eqn4)}$$

3. Results

3.1. Composition of fish schools

Gas-filled scatterer aggregations in the water column detected using the EK60 vessel-based echosounder in October 2016 and January 2017 were mostly juvenile sprat *S. sprattus* and some whiting *Merlangius merlangus* according to the trawl samples (Figure 3, see Appendix S2).

3.2. Behaviour of fish schools

Diel vertical migration (DVM) of schools were detected by both the bottom deployed AZFP and the vessel mounted EK60 echo sounder. EK60 transect surveys showed spatial distribution and relative density (nautical area scattering coefficient s_A) of swim bladdered fish schools undertaking DVM were random (Moran's I indexes for surveys $P > .05$) and temporally variable across the Holyhead Deep project area in both October 2016 and January 2017.

The bottom deployed AZFP showed schools of swim bladdered fish, that trawls indicated to be mainly composed of sprat, were present in all months of the study with 20,858 schools detected from 12:00 8th October 2016 to 12:00 on 20th January 2017. The mean hourly school height (bottom of school to top of school) was 1.28 m ± 0.51 (sd). These schools were not detected before 05:00 local time neither after 18:00. Fish schools undertook DVM throughout the entire study. Schools would form and descend from the surface in the morning, and then ascend back towards the surface and disperse in the evening (Figure 5). The deepest hourly mean school depth was 49.67 m with a mean depth of 19.01 ± 8.5 m (sd).

3.3. Behaviour drivers

3.3.1. Relationships between school depth and physical properties

Daily mean depth of DVM fish schools show a cyclical trend of reaching maximum and minimum depths every 2 weeks (Figure 6), with periods of significant ($\alpha = 0.05$) positive autocorrelation (max lag of 60 days) peaking at lags of 15 and 29 days. The daily median SPM size (D50) had significant positive peaks at 15, 29 and 44 days, median tidal current magnitude 15, 29, 45 and 59 days and maximum irradiance depth at 14 and between 27 and 31 days. Daily median SPM TVC had peaks in significant positive autocorrelation 30 and 60 days. These same variables were significantly correlated (Spearman's Rank r_s, $\alpha = 0.05$) with the daily mean DVM fish school depth, with the maximum irradiance depth (r_s 0.78) and SPM D50 (0.80) being positively correlated, median tidal current speed (r_s -0.64) and SPM TVC (r_s -0.58) being negatively correlated (Figure 7). The observed range in fish school depths between 10:00 and 14:00 each day did not show any correlation with the daily range in irradiance depth each day (r_s -0.12) or current speed (r_s -0.09).

Multiple linear regression produced significant relationships between median daily DVM fish school depth and daily maximum irradiance depth ($P < .001$), daily median tidal current magnitude ($P < .001$) and daily mean total volume concentration of SPM ($P < .001$). The model with these three predictor variables accounted for 78% (adjusted R^2) of the variation with assumptions of residual normality and homogeneity of variance and linearity met, with variance inflation factor analysis indicating acceptable predictor variable multicollinearity after the removal of median SPM D50 and mean solar radiation from the model. Separate linear regression models with only daily median D50 and daily maximum irradiance depth produced significant fits (both $P < .001$) explaining 63% and 60% of the variation in daily median DVM respectively, and 74% when both in the regression model. Median tidal magnitude only accounted for 41% of the variation when the only predictor variable in the model ($P < .001$).

Time series analysis, using seasonal-trend decomposition by regression, of the mean daily DVM school depth indicate an overall trend of a deeper ~ 22 m depth distribution in October shifting to a ~ 15 m depth distribution in December and January, mainly shallowing during November. This analysis detected 14 and 29 day cycles that had similar importance for the observed school depths, with its

influence diminishing during the study period, with unexplained variation dominating in January above the lunar cycles. The time series analysis revealed similar trends in irradiance depth.

3.3.2. SPM and Tidal currents

Observed current speed showed a maximum of 2.19 m s^{-1} and a mean ±1 sd of 0.92 ±0.48 m s^{-1} (Figure 6). Strong tidal asymmetry can be seen between flood and ebb currents (Figure 5d). On a longer temporal scale, tidal currents show a spring-neap variation, during new moon and full moon phases tidal currents are greatest, representing spring tidal currents, and during first or third quarter phases they are smallest, representing neap tidal currents (Figure 6). Results show TVC and D50 are correlated to current speed (Figure 7) on tidal and spring-neap time scales (Figure 6). Particle size is greatest when current speeds are at a minimum, during high water slack and low water (Figure 5) and during neap tides (Figure 6). On a spring-neap time scale, TVC and current speed are positively correlated, most likely due to a combination of advection and resuspension of local sediments (Figure 6). Median particle size presents an inverse relationship with current speed (Figure 7) with larger sizes for D50 occurring during neap tides, when current speeds are weakest (Figure 6).

3.4. DVM fish school and MRE device overlap

When DVM fish schools were present a mean daily proportion of time overlapping with potential kite operations (PO_{FS}) was 0.08 for both 8th – 31st of October and the whole of November, with and January 1st – 20th having a mean potential overlap of 0.02 (Figure 6c). Typically periods of overlap occurrence were one to four days in duration (Figure 6c), with the exception of a new moon spring tide (lower current speeds and fish remaining deeper than preceding and following full moon spring tides) at the end of October into November, when 10 consecutive days of overlap occurred, peaking with a day of 0.36 overlap. October (24 days sampled) and November (30 days sampled) had 10 and 11 days with overlap occurrence respectively. In contrast, December (31 days sampled) and January (20 days sampled) had 4 and 3 days where overlap occurred respectively (Figure 6c).

This 0.05 proportion of time DVM fish schools are overlapped by kite flying operations (PO_{FS}), represents a mean daily proportion of 0.06 of the total time the kite would be operating (PO_k) over the study period, with the highest mean overlap for a single day being 0.44. When averaged over each month of the study period the mean daily proportion of total kite operating time overlapped by fish schools decreased from 0.10 (maximum for a day 0.40) and 0.09 (maximum for a day 0.44) over October and November respectively, to 0.02 in both December (maximum for a day 0.33) and January (maximum for a day 0.17).

4. Discussion

This study observed fish schools (trawls indicate to be dominated by sprat) undertaking DVM in the Holyhead Deep. The depth reached by the schools varied, with greater depths reached every two weeks correlating (in descending order of correlation strength) with larger D50 values, deeper light penetration into the water column, lower daily tidal currents speeds during neap tides and lower SPM concentrations. During the study period there was a trend of decreasing school depths from autumn into winter, with evidence that lunar cycles driving the tidal spring-neap cycle reduced in correlation with DVM in December and January when compared with October and September. This shallowing of fish schools with time, probably due to reduced solar radiation at the sea surface reducing the depth of light penetration, produced a reduction in the proportion of overlap between the fish schools and the DG500 tidal energy kite. Our findings have implications for management authorities and MRE device developers in assessing and potentially mitigating environmental impacts of marine renewable projects, enabling a comparison of different MRE designs, operating depths and operating envelopes that may alter the duration of possible interactions with marine fauna.

The proportion of overlap calculated in this study is based on the DVM schools occurring between 20 and 60 m depth when the kite would be operational (based on current speed) only, and does not take into account the dimensions of the kite, the positive relationship between kite speed with tidal current speed, the dimensions and spacing of fish schools or any possible avoidance behaviour of fish schools.

Therefore, the proportion calculated is a 'worst case scenario', which shows general trends and variations in magnitudes of potential overlap. In addition, the presence of DVM schools may be underestimated at dawn and dusk due to fish schools being close to the surface making detection less likely, especially when surface turbulence is present, which may inflate calculated PO_{FS} but have not effect on PO_k.

Peaks in proportion of overlap between the kite and DVM fish schools did not occur during days when fish schools were migrating deepest, as might be expected. This was due to fish schools migrating deeper when turbidity was lower (lower TVC and larger D50), which occurs during neap-tides with lower current velocities when the kite cut-in speed of 1.2 m s^{-1} is reached infrequently, and so the kite would not be operating for long periods. However, during the transition between neap tides to spring tides the fish schools were in the kite operating depth, despite migration depth becoming shallower, and the kite cut-in speed was now met more often resulting in overlap with kite operation and fish schools for longer periods of time. The longest period of overlap occurred for ten consecutive days at the end of October into the start of November, and was during a new moon spring tide when the schools were 'shallow' compared with a neap tide, but still migrating to average depths greater than 20 m when current speeds were > 1.2 m s^{-1} for consistent periods of time. The low count of overlap days and proportion of overlap in December and January was driven by the DVM fish schools remaining shallower and not being present for as long each day as day length decreased. Due to the seasonal variation observed, caution should be given to extrapolating any results beyond the sampled time period. Fish have been shown to potentially modify their behaviour in the presence of marine renewable devices in other development areas (Fraser et al., 2018; Viehman & Zydlewski, 2015), and so work is currently underway to understand how schools may react to an operating tidal kite.

DVM of sprat schools has been observed in fjords (Knudsen, Hawkins, McAllen, & Sand, 2009) and the Baltic Sea (Nilsson, 2003), and here in an open marine coastal system of the Holyhead Deep. Due to the mixed water column in the Holyhead Deep, the 'antipredation window' (Clark & Levy, 1988) determined by the depth variation in light irradiance would appear a key driver of these vertical migrations, as opposed to temperature or dissolved oxygen levels influencing migratory behaviour in

more sheltered and stratified systems (Solberg & Kaartvedt, 2017). This study has shown that the magnitude of fish school DVM can change in correlation with the spring-neap tidal cycle, due to its influence on irradiance depth in the water column.

Sprat schools may afford better protection during spring tides through the higher turbidity as the distance at which their predators can detect them, termed reactive distance, is reduced (De Robertis et al., 2003), while theirs is impacted less due to foraging on zooplankton prey at much closer ranges. However, the sprat are not migrating as deep during spring tides due to the restricted light penetration, which may increase the number of predator species that can reach them and the duration that predators can forage for, potentially overriding any survival advantage of higher turbidity. Neap tides will increase reactive distance for foraging sprat and their predators due to lower turbidity (lower TVC and larger D50, resulting a lower SPM cross-sectional area), but surface diving predators (visual, tactile and acoustic hunters) would need to reach greater depths with potentially higher energetic cost. An interesting question on the implications of our results on surface diving visual predators is whether reactive distance, mediated by the turbidity, is more important for predators foraging on sprat schools than the depth of prey during the day. Cormorants for example have short reactive distances of < 1 m even in low turbidity water (White, Day, Butler, & Martin, 2007), and may benefit from shallow schools during turbid spring tides more than greater reactive distance when feeding on deeper prey during neap tides. In contrast, visibility may be more limiting for species that have greater reactive distances, and so forage more successfully during neap tides despite prey being deeper.

Gannets (Brierley & Fernandes, 2001) and Manx shearwater (Shoji et al., 2016) do not routinely dive to depths greater than 20 m, but are capable of reaching depths of 34 m and 55 m respectively. Other species capable of diving between 20 and 60 m include the common guillemot, puffin and razorbill (Langton, Davies, & Scott, 2011). Common guillemots/murres *Uria aalge* were the most frequently sighted species of seabird in the Holyhead Deep in September 2016 (Jackson, 2017) and are known to feed on juvenile sprat and whiting (Anderson, Evans, Potts, Harris, & Wanless, 2014; Riordan & Birkhead, 2018). Common guillemots' diving behaviour can follow the DVM of their prey (Regular, Davoren, Hedd, & Montevecchi, 2010), and so the predicted proportion of overlap of fish school prey

with the kite in this study could be similar and a proxy for the potential overlap between common guillemots and the tidal kite. However, if foraging of diving visual predators focuses on the dawn and dusk descent and ascent phase (Dean et al., 2012; Garthe, Montevecchi, & Davoren, 2007; Regular et al., 2010) then the implications of the school layer depth during the majority of the day would be diminished.

Conclusions

We suggest that the depth of light penetration into the water column, calculated using a new method, may predictably determine the depth of DVM undertaken by sprat schools in the Holyhead Deep. Our results show that the depth of light penetration is influenced by the predictable, yet still seasonally variable, SPM dynamics. We show that these SPM properties are strongly influenced by the lunar cycle of tidal current speeds, which are highly relevant in areas of MRE development. Therefore, the temporal dynamics of SPM play an important role in determining potential overlap between MRE devices such as the DG500 kite and fish schools, and the predators potentially foraging on them. This finding shows that single or less than seven day sampling campaigns can miss important behaviour of fish that may alter interaction predictions with MRE devices, and that changes to SPM dynamics from MRE developments may have ecosystem implications. As demonstrated in this study, understanding the behaviour of top predator's prey species at MRE sites gives developers and environmental managers valuable information for predicting potential impacts, and comparing different MRE devices designs and operating characteristics. In addition, our findings have implications for understanding constraints on top predator foraging opportunities and use of high current areas.

Authors' contributions

TW conceived the idea; TW, SJ, JH, BS, BP, AD and LG designed the methodology; TW, SJ, BP and TDJ collected the data; TW, SJ, and DB analysed the data; TW and SJ led the writing of the manuscript with BS and JH contributing critically to the drafts; all authors gave final approval for publication.

Acknowledgements

This work was part of the SEACAMS2 project part-funded by the European Regional Development Fund through the Welsh Government. We would like to thank Minesto UK Ltd. for their collaboration and support. The authors are grateful to the crew of the RV Prince Madog, Jenny Bond, Serena Teasdale, Jonathan Demmer, Aled Owen, Michael Roberts, Shunya Hashiguchi, Sarah Louise Jones and Peter Hughes for help with sampling at sea. We also thank Jan Buermans and David Lemon at ASL for use of the AZFP, Welsh Government fisheries for permission to land trawl catches, Crown Estate for permission to deploy moorings onto the seabed and the National Meteorological Library and Archive – Met Office, UK for solar radiation values. We thank two anonymous reviewers for helpful comments on an earlier version of the manuscript.

Data Availability Statement

Data available via figshare repository https://dx.doi.org/10.6084/m9.figshare.11671740.v1 (Whitton et al., 2020).

References

Anderson, H. B., Evans, P. G. H., Potts, J. M., Harris, M. P., & Wanless, S. (2014). The diet of Common Guillemot Uria aalge chicks provides evidence of changing prey communities in the North Sea. *Ibis*, *156*(1), 23–34. doi: 10.1111/ibi.12099

Baptist, M. J., & Leopold, M. F. (2010). Prey capture success of Sandwich Terns Sterna sandvicensis varies non-linearly with water transparency. *Ibis*, *152*(4), 815–825. doi: 10.1111/j.1474-919X.2010.01054.x

Benoit-Bird, K. J., & Lawson, G. L. (2016). Ecological Insights from Pelagic Habitats Acquired Using Active Acoustic Techniques. *Annual Review of Marine Science*, *8*(1), 463–490. doi: 10.1146/annurev-marine-122414-034001

Bianchi, D., & Mislan, K. A. S. (2016). Global patterns of diel vertical migration times and velocities from acoustic data. *Limnology and Oceanography*, *61*(1), 353–364. doi: 10.1002/lno.10219

Brierley, A. S., & Fernandes, P. G. (2001). Diving Depths of Northern Gannets: Acoustic Observations of Sula Bassana from an Autonomous Underwater Vehicle. *The Auk*, *118*(2), 529–534. doi: 10.1642/0004-8038(2001)118

Clark, C. W., & Levy, D. A. (1988). Diel Vertical Migrations by Juvenile Sockeye Salmon and the Antipredation Window. *The American Naturalist*, *131*(2), 271–290. doi: 10.1086/284789

De Robertis, A., & Handegard, N. O. (2013). Fish avoidance of research vessels and the efficacy of noise-reduced vessels: a review. *ICES Journal of Marine Science*, *70*(1), 34–45. doi: 10.1093/icesjms/fss155

De Robertis, A., Ryer, C. H., Veloza, A., & Brodeur, R. D. (2003). Differential effects of turbidity on prey consumption of piscivorous and planktivorous fish. *Canadian Journal of Fisheries and Aquatic Sciences*, *60*(12), 1517–1526. doi: 10.1139/f03-123

Dean, B., Freeman, R., Kirk, H., Leonard, K., Phillips, R. A., Perrins, C. M., & Guilford, T. (2012). Behavioural mapping of a pelagic seabird: combining multiple sensors and a hidden Markov model reveals the distribution of at-sea behaviour. *Journal of The Royal Society Interface*, *10*(78), 20120570–20120570. doi: 10.1098/rsif.2012.0570

Demer, D. A., Berger, L., Bernasconi, M., Bethke, E., Boswell, K. M., Chu, D., … Williamson, N. (2015). *Calibration of acoustic instruments. ICES Cooperative Research Report No.326*. Retrieved from http://ices.dk/sites/pub/Publication Reports/Cooperative Research Report (CRR)/crr326/CRR326.pdf

Dokumentov, A., & Hyndman, R. J. (2018). *stR: STR Decomposition. R. package version 0.4*. Retrieved from https://cran.r-project.org/package=stR

Fernandes, P. G. (2009). Classification trees for species identification of fish-school echotraces. *ICES Journal of Marine Science*, *66*(6), 1073–1080. doi: 10.1093/icesjms/fsp060

Fraser, S., Williamson, B. J., Nikora, V., & Scott, B. E. (2018). Fish distributions in a tidal channel indicate the behavioural impact of a marine renewable energy installation. *Energy Reports*, *4*,

65–69. doi: 10.1016/j.egyr.2018.01.008

Garthe, S., Montevecchi, W. A., & Davoren, G. K. (2007). Flight destinations and foraging behaviour of northern gannets (Sula bassana) preying on a small forage fish in a low-Arctic ecosystem. *Deep Sea Research Part II: Topical Studies in Oceanography*, *54*(3–4), 311–320. doi: 10.1016/j.dsr2.2006.11.008

Granqvist, M., & Mattila, J. (2004). The effects of turbidity and light intensity on the consumption of mysids by juvenile perch (Perca fluviatilis L.). *Hydrobiologia*, *514*, 93–101.

Irigoien, X., Conway, D., & Harris, R. (2004). Flexible diel vertical migration behaviour of zooplankton in the Irish Sea. *Marine Ecology Progress Series*, *267*, 85–97. doi: 10.3354/meps267085

Jackson, D. (2017). *Minesto Deep Green ESAS Survey Summary: August to September 2016 and March to May 2017*.

Kimbell, H. S., & Morrell, L. J. (2015). Turbidity weakens selection for assortment in body size in groups. *Behavioral Ecology*, arv183. doi: 10.1093/beheco/arv183

Knudsen, F. R., Hawkins, A., McAllen, R., & Sand, O. (2009). Diel interactions between sprat and mackerel in a marine lough and their effects upon acoustic measurements of fish abundance. *Fisheries Research*, *100*(2), 140–147. doi: 10.1016/j.fishres.2009.06.015

Langton, R., Davies, I. M., & Scott, B. E. (2011). Seabird conservation and tidal stream and wave power generation: Information needs for predicting and managing potential impacts. *Marine Policy*, *35*(5), 623–630. doi: 10.1016/j.marpol.2011.02.002

Lee, H., Kang, D., & Choi, J. W. (2015). The effect of the suspended solid concentration on the daytime vertical distribution of Euphausia pacifica in the Yellow Sea, Korea. *Fisheries Science*, *81*(5), 849–859. doi: 10.1007/s12562-015-0904-5

Nilsson, L. (2003). Vertical migration and dispersion of sprat (Sprattus sprattus) and herring (Clupea harengus) schools at dusk in the Baltic Sea. *Aquatic Living Resources*, *16*(3), 317–324. doi:

10.1016/S0990-7440(03)00039-1

Oozeki, Y., Hu, F., Kubota, H., Sugisaki, H., & Kimura, R. (2004). Newly designed quantitative frame trawl for sampling larval and juvenile pelagic fish. *Fisheries Science*, *70*(2), 223–232. doi: 10.1111/j.1444-2906.2003.00795.x

Piano, M., Lewis, M., Ward, S., Robins, P., Lewis, M., Davies, A. G., & Powell, B. (2015). Characterizing the tidal energy resource of the West Anglesey Demonstration Zone (UK), using TELEMAC-2D and field observations Characterizing the tidal energy resource of the West Anglesey Demonstration Zone (UK), using TELEMAC-2D and field observatio. In C. Moulinec & D. Emerson (Eds.), *Proceedings of the XXII TELEMAC-MASCARET Technical User Conference October 15-16* (pp. 195–203). Retrieved from https://henry.baw.de/bitstream/20.500.11970/104333/1/30_Piano_2015.pdf

R Core Team. (2019). R: A language and environment for statistical computing. *R Foundation for Statistical Computing*. Retrieved from https://www.r-project.org

Regular, P., Davoren, G., Hedd, A., & Montevecchi, W. (2010). Crepuscular foraging by a pursuit-diving seabird: tactics of common murres in response to the diel vertical migration of capelin. *Marine Ecology Progress Series*, *415*, 295–304. doi: 10.3354/meps08752

Riordan, J., & Birkhead, T. (2018). Changes in the diet composition of Common Guillemot Uria aalge chicks on Skomer Island, Wales, between 1973 and 2017. *Ibis*, *160*(2), 470–474. doi: 10.1111/ibi.12570

Robison, B. H. (2003). What drives the diel vertical migrations of Antarctic midwater fish? *Journal of the Marine Biological Association of the United Kingdom*, *83*(3), 639–642. doi: 10.1017/S0025315403007586h

Roche, R. C., Walker-Springett, K., Robins, P. E., Jones, J., Veneruso, G., Whitton, T. A., … King, J. W. (2016). Research priorities for assessing potential impacts of emerging marine renewable energy technologies: Insights from developments in Wales (UK). *Renewable Energy*, *99*, 1327–

1341. doi: 10.1016/j.renene.2016.08.035

Scrope-Howe, S., & Jones, D. (1986). The vertical distribution of zooplankton in the western Irish Sea. *Estuarine, Coastal and Shelf Science*, *22*(6), 785–802. Retrieved from http://www.sciencedirect.com/science/article/pii/0272771486900995

Shoji, A., Dean, B., Kirk, H., Freeman, R., Perrins, C. M., & Guilford, T. (2016). The diving behaviour of the Manx Shearwater Puffinus puffinus. *Ibis*, *158*(3), 598–606. doi: 10.1111/ibi.12381

Solberg, I., & Kaartvedt, S. (2017). The diel vertical migration patterns and individual swimming behavior of overwintering sprat Sprattus sprattus. *Progress in Oceanography*, *151*, 49–61. doi: 10.1016/j.pocean.2016.11.003

Viehman, H. A., & Zydlewski, G. B. (2015). Fish Interactions with a Commercial-Scale Tidal Energy Device in the Natural Environment. *Estuaries and Coasts*, *38*(S1), 241–252. doi: 10.1007/s12237-014-9767-8

Vinyard, G. L., & O'brien, W. J. (1976). Effects of Light and Turbidity on the Reactive Distance of Bluegill (Lepomis macrochirus). *Journal of the Fisheries Research Board of Canada*, *33*(12), 2845–2849. doi: 10.1139/f76-342

Weeks, A. R., Simpson, J. H., & Bowers, D. (1993). The relationship between concentrations of suspended particulate material and tidal processes in the Irish Sea. *Continental Shelf Research*, *13*(12), 1325–1334. doi: 10.1016/0278-4343(93)90086-D

Westgate, A. J., Head, A. J., Berggren, P., Koopman, H. N., & Gaskin, D. E. (1995). Diving behaviour of harbour porpoises, *Phocoena phocoena*. *Canadian Journal of Fisheries and Aquatic Sciences*, *52*(5), 1064–1073. doi: 10.1139/f95-104

White, C. R., Day, N., Butler, P. J., & Martin, G. R. (2007). Vision and Foraging in Cormorants: More like Herons than Hawks? *PLoS ONE*, *2*(7), e639. doi: 10.1371/journal.pone.0000639

Whitton, T. A., Jackson, S. E., Hiddink, J. G., Scoulding, B., Bowers, D., Powell, B., … Davies, A. G.

(2020). Data from: Vertical migrations of fish schools determine overlap with a mobile tidal stream marine renewable energy device. figshare repository https://dx.doi.org/10.6084/m9.figshare.11671740.v1

Williamson, B. J., Fraser, S., Blondel, P., Bell, P. S., Waggitt, J. J., & Scott, B. E. (2017). Multisensor Acoustic Tracking of Fish and Seabird Behavior Around Tidal Turbine Structures in Scotland. *IEEE Journal of Oceanic Engineering, 42*(4), 948–965. doi: 10.1109/JOE.2016.2637179

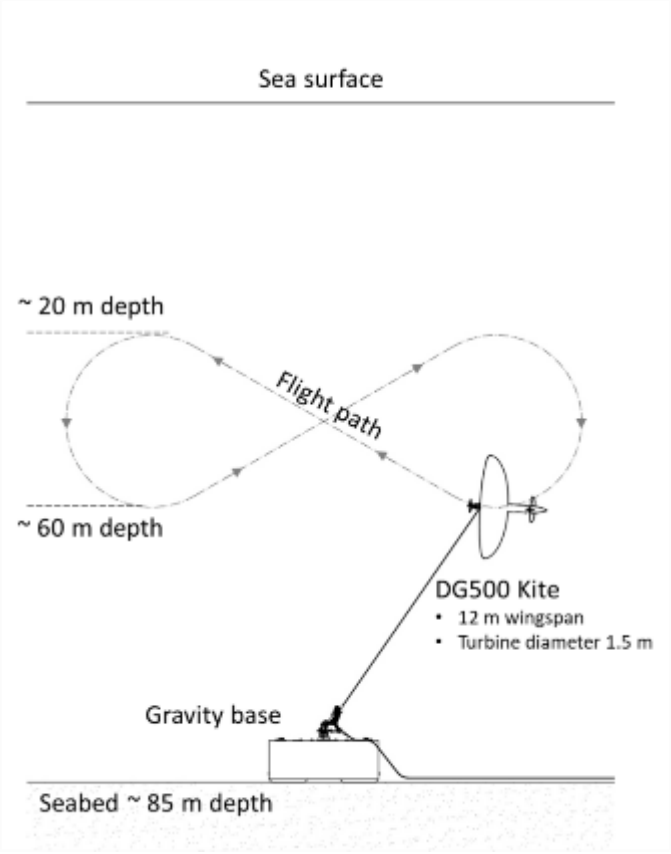

Figure 1. The Minesto DG500 tidal kite consists of a wing and turbine directly coupled to a generator in a nacelle. Rudders steer the kite in the predetermined figure of eight trajectory perpendicular to the tidal current direction. The kite is connected to a tether that is connected to a bottom joint at the gravity base seabed foundation. The tether accommodates the tether rope and cables for communication and power distribution. The figure of eight flight path will cover approximately 20 – 60 m depth range with a 100 m horizontal span. Adapted from image provided by Minesto UK Ltd.

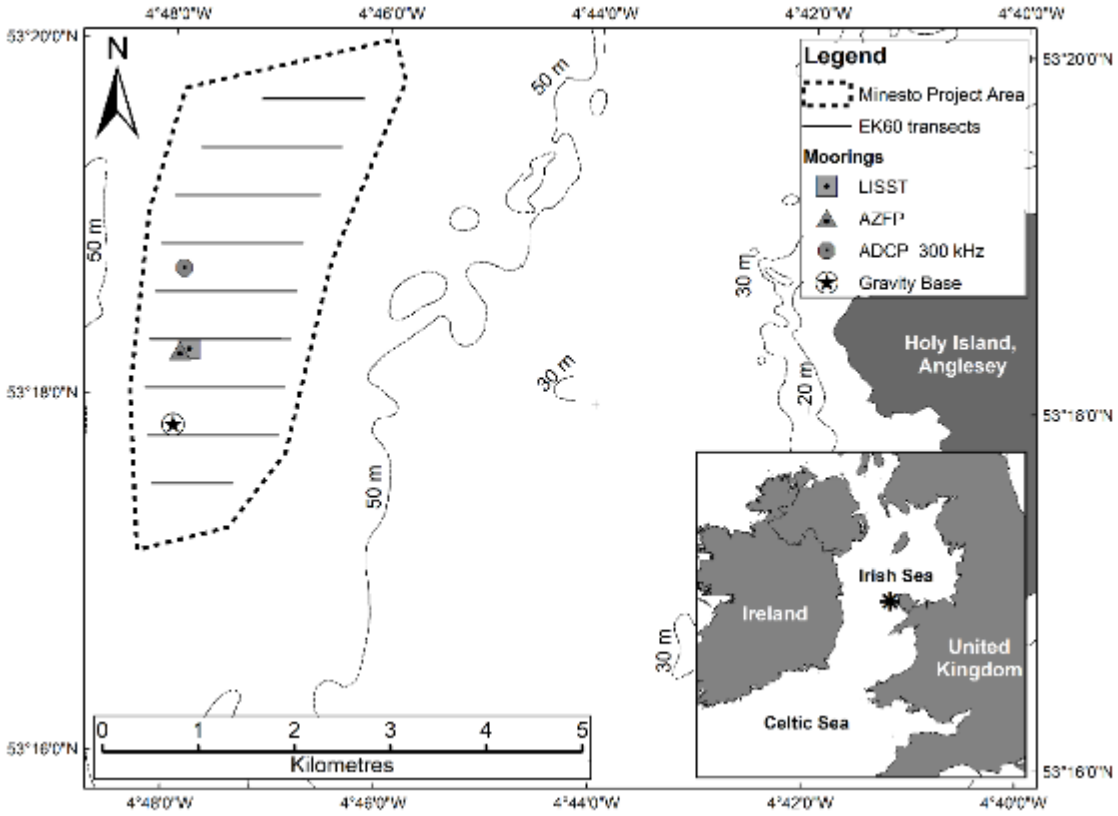

Figure 2. Map of the Holyhead Deep Minesto UK Ltd. lease area (thick dashed line) off the west coast of Holy Island, UK showing mooring locations and EK60 echosounder transects (solid black line) surveyed in October 2016 and January 2017. The instrument moorings, which included an Acoustic Zooplankton Fish Profiler (AZFP), a laser in situ scattering and transmissometer (LISST), and an Acoustic Doppler Current Profiler (ADCP), were deployed at a depth of around 85 m on the 1st and 2nd of October 2016, and recovered on 26th January 2017. The Gravity base shows the location of the kite deployment location in 2018 subsequent to this study. The 20, 30 and 50 m depth contours are shown by the thin dashed lines. Asterisk in inset map shows location of main Holyhead Deep within the Irish Sea.

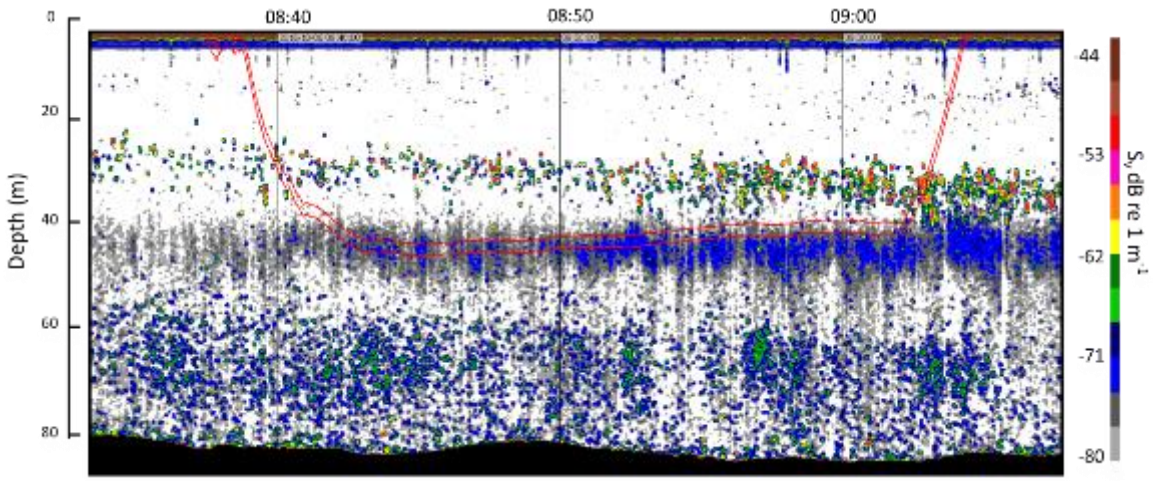

Figure 3. Example daytime mid-water trawl profile from 6th October 2016 (corrected for mean layback) overlaid on EK60 120 kHz acoustic backscatter (each sample is a 50 cm depth by 5 second average to aid visualisation) collected during trawls to sample scattering layer at 40 – 50 m depth, identified as mostly containing northern krill *Meganyctiphanes norvegica* that increases in density during the trawl. Schools of sprat *Sprattus sprattus* can be seen above the krill layer at 20 – 40 m depth as yellow to red blobs, again becoming denser and also increasing in depth during the trawl period. Mixed species scattered targets can be seen below the krill scattering layer from 60 m to the seabed.

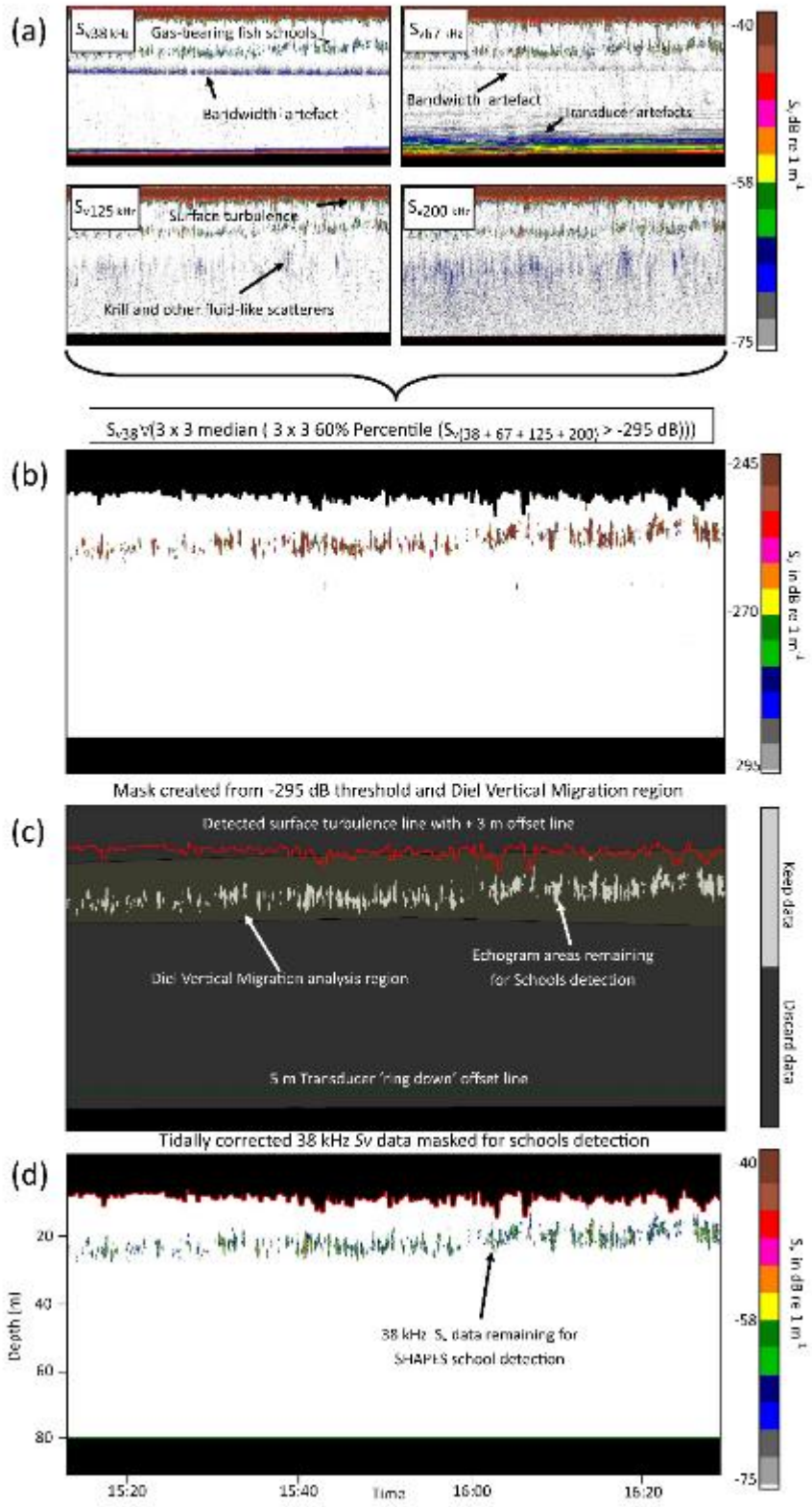

Figure 4. Analysis workflow for detecting fish schools undertaking diel vertical migrations (DVM) using an ASL Acoustic Zooplankton and Fish Profiler (AZFP). Panel (a) shows example raw echograms of the 38, 67, 125 and 200 kHz data spanning an hour on 3rd November 2016 that include other sources

of biological backscatter (such as northern krill) and instrument associated noise including a bandwidth artefact clearly seen on the 38 kHz frequency echogram (a). The algorithm shown was used to (b) isolate backscatter from swim bladdered fish within a (c) DVM migration region and analysis exclusion lines below surface turbulence and above the transducer ring down region. The mask produced from these steps (c) was applied to (d) the raw 38 kHz S_v (Volume backscattering strength dB re 1 m^{-1}) backscatter at a threshold of -75 dB, and schools subsequently detected using a SHAPES algorithm.

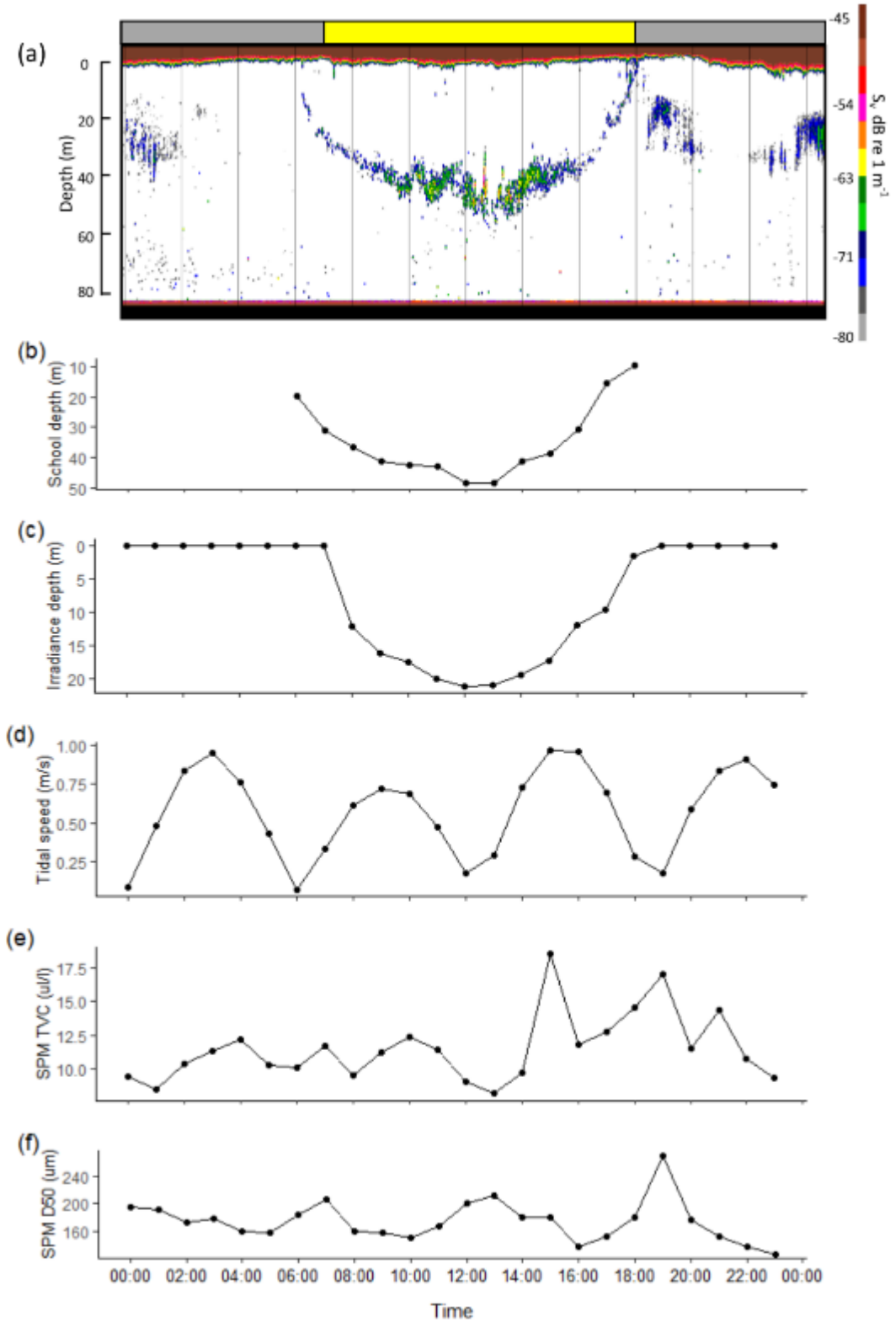

Figure 5. Measurements collected and calculated for the 11th October 2016 by the bottom mounted AZFP (Acoustic, Zooplankton and Fish Profiler) deployed in the Holyhead Deep, UK. a) DVM (Diel Vertical Migration) of swim bladdered fish can be seen in the acoustic backscatter* with grey and tallow

bars indicating times of zero and positive detected global solar radiation respectively, b) hourly mean school depths between 06:00 and 18:00. The c) diel pattern in light penetration (calculated depth of 10 MJ hr^{-1}) can be seen with the semidiurnal variation in d) tidal current speed in the ADCP (Acoustic Doppler Current Profiler). Calibrated e) TVC (Total Volume Concentration) and f) D50 (Median particle size) were recorded 8 m above the seabed by a LISST (Laser In Situ Scattering and Transmissometry) instrument.*A three sample by 60 ping (three minute) averaging of the 38 kHz backscatter has been applied to the data to more clearly show the migration over 24 hours.

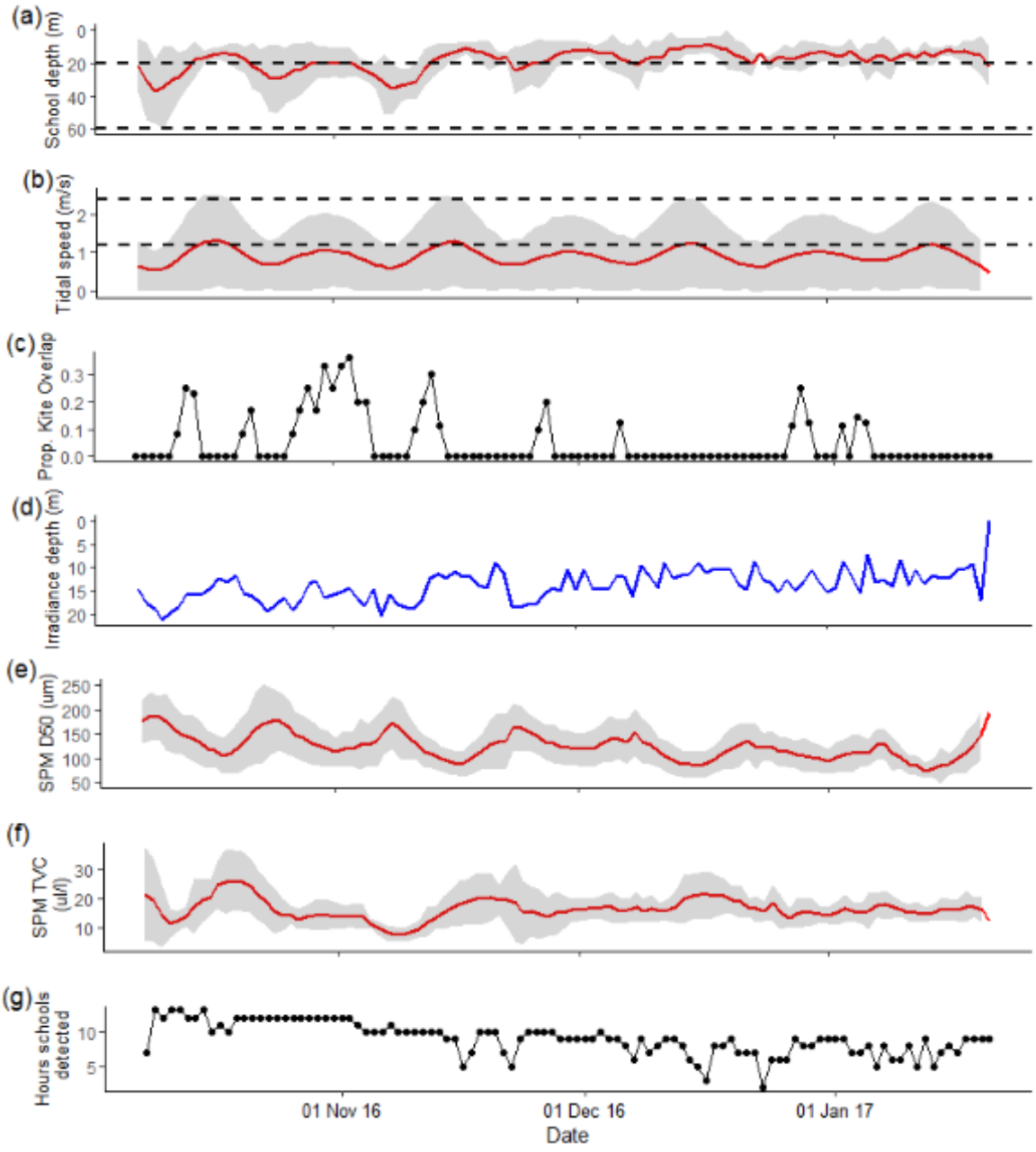

Figure 6. Daily average (red line, with grey ribbon showing ± one standard deviation) of a) depth of fish schools undertaking DVM, b) tidal current from the deployed ADCP, and c) the daily proportion of overlap between detected fish schools and a tidal energy kite when operating between 20 – 60 m depth (dashed lines in panel (a)) and at kite operating threshold current speeds between 1.2 m s^{-1} and 2.4 m s^{-1} (dashed lines in panel (b)) for the Holyhead Deep from 12:00 on 08/10/2016 to 00:00 on 20/01/2017. The d) predicted daily maximum irradiance depth was calculated utilising the e) median particle size (D50) and f) total volume concentration (TVC) collecting by the LISST. The g) daily count of hours in which DVM fish schools were detected are also shown.

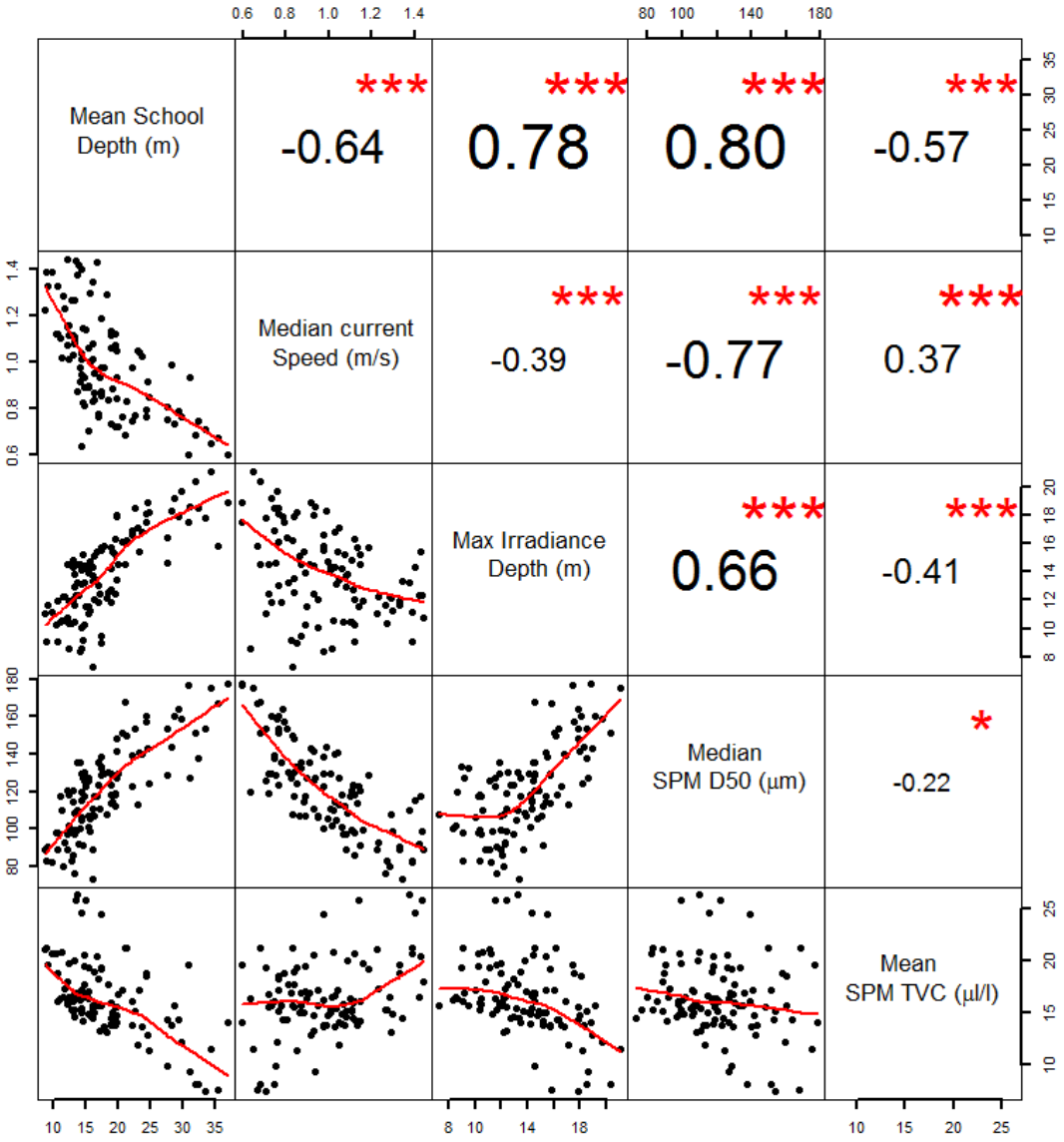

Figure 7. Relationship and Spearman's rank (r_s) correlation of the mean DVM school depth and the key physical variables. Numbers show the r_s coefficient and * indicates a significance at $P \leq .05$ and *** at $P \leq .001$. Red best-fit line illustrates relationship trend.